frontiers | Frontiers in Marine Science

TYPE Original Research
PUBLISHED 23 October 2024
DOI 10.3389/fmars.2024.1466037

OPEN ACCESS

EDITED BY
Jianchuan Yin,
Guangdong Ocean University, China

REVIEWED BY
Sarat Chandra Tripathy,
National Centre for Polar and Ocean Research (NCPOR), India
Guifen Wang,
Hohai University, China

*CORRESPONDENCE
David Antoine
david.antoine@curtin.edu.au

RECEIVED 17 July 2024
ACCEPTED 24 September 2024
PUBLISHED 23 October 2024

CITATION
Li J, Antoine D and Huot Y (2024) Bio-optical variability of particulate matter in the Southern Ocean.
Front. Mar. Sci. 11:1466037.
doi: 10.3389/fmars.2024.1466037

Bio-optical variability of particulate matter in the Southern Ocean

Juan Li[1,2], David Antoine[1,2]* and Yannick Huot[3]

[1]Remote Sensing and Satellite Research Group, School of Earth and Planetary Sciences, Curtin University, Perth, WA, Australia, [2]Australian Research Council (ARC) Australian Centre for Excellence in Antarctic Science (ACEAS), University of Tasmania, Hobart, TAS, Australia, [3]Centre d'Applications et de Recherches en Télédétection, Département de géomatique appliquée, Université de Sherbrooke, Sherbrooke, QC, Canada

The composition and size distribution of particles in the ocean control their optical (scattering and absorption) properties, as well as a range of biogeochemical and ecological processes. Therefore, they provide important information about the pelagic ocean ecosystem's structure and functioning, which can be used to assess primary production, particle sinking, and carbon sequestration. Due to its harsh environment and remoteness, the particulate bio-optical properties of the Southern Ocean (SO) remain poorly observed and understood. Here, we combined field measurements from hydrographic casts from two research voyages and from autonomous profiling floats (BGC-Argo) to examine particulate bio-optical properties and relationships among several ecologically and optically important variables, namely the phytoplankton chlorophyll *a* concentration (Chl), the particulate absorption coefficient (a_p), the particulate backscattering coefficient (b_{bp}), and the particulate organic carbon (POC) concentration. In the clearest waters of the SO (Chl < 0.2 mg m^{-3}), we found a significant contribution to absorption by non-algal particles (NAP) at 442 nm, which was up to 10 times greater than the absorption by phytoplankton. This makes the particulate bio-optical properties there remarkably different from typical oceanic case 1 water. A matchup analysis confirms the impact of this larger NAP absorption on the retrieval of Chl from satellite ocean colour observations. For waters with Chl > 0.2 mg m^{-3}, no significant differences are observed between the SO and temperate waters. Our findings also demonstrate consistency in predicting phytoplankton carbon from either Chl or b_{bp}, suggesting that both methods are applicable in the SO.

KEYWORDS

Southern Ocean, particles, bio-optical properties, bio-optical relationships, BGC-Argo floats

1 Introduction

In the sunlit upper ocean, autotrophic organisms take up CO_2 and utilise inorganic nutrients via photosynthesis to produce organic matter, packaged in the form of phytoplankton cells, that accumulates in the water column as suspended particles (Falkowski et al., 1998). These phytoplankton cells provide energy for essentially the entire pelagic ecosystem and are, thereby, transformed into a large variety of living and nonliving particles through a myriad processes: viral infection, shedding of vesicles and other cellular parts, grazing by zooplankton (Jackson, 1980; Steinberg and Landry, 2017; Karakuş et al., 2022), remineralisation by microbes (Boyd et al., 2015; Belcher et al., 2016; Cavan et al., 2017), and (dis)aggregation by a series of biogeophysical and biogeochemical processes (Jackson and Burd, 1998; Slade et al., 2011; Briggs et al., 2020). A fraction of their accumulated carbon and nutrients eventually sinks (or is advected) into deep unlit layers as part of the so-called biological pump (Buesseler et al., 2007; Turner, 2015; Boyd et al., 2019). The particle flux and its composition in the water column represent a dynamic balance between ecosystem-driven processes that generate large sinking particles in the upper ocean and particle recycling processes within the ocean interior that consume, modify, and produce new sinking particles (Clements et al., 2022). Therefore, marine particles are critical in the characterisation of pelagic ecosystems, as they control a range of biogeochemical and ecological processes, and influence the ability of the ocean to sequester carbon.

The Southern Ocean (SO) is responsible for ~ 40% of the global oceanic CO_2 uptake (Gruber et al., 2009) and is a key driver of global ocean circulation and climate (Stark et al., 2019). Characterising and understanding particle dynamics in the surface layer is particularly important for assessing the strength of the biological pump under the pressure of climate change. However, the remoteness and difficult field conditions limit the opportunities for *in situ* studies of the SO. In this context, ocean colour remote sensing (OCRS) can provide a powerful tool to monitor it and obtain spatially resolved information. However, given the importance of the SO in oceanic carbon uptake and productivity, estimates must be accurate, as any error will have a large impact on our ability to obtain global estimates. In turn, for remote sensing to be accurate, we must determine whether global relationships derived elsewhere between satellite-measured quantities—such as spectral remote sensing reflectance or normalised water-leaving radiance—and *in situ* variables are applicable in the SO. This need has spurred studies examining the particulate bio-optical properties and relationships in the SO.

Allison et al. (2010a) found a different relationship between particulate organic carbon (POC) and the blue-to-green band ratios of reflectance in the SO compared to other oceans, such as the North Polar Atlantic (Stramska et al., 2003) and the eastern South Pacific and eastern Atlantic oceans (Stramski et al., 2008). Their new relationship has been applied to satellite observations to characterise the seasonal and interannual variability of POC in the SO (Allison et al., 2010b). Johnson et al. (2013) have reported three improved satellite chlorophyll algorithms for the SO to better monitor phytoplankton dynamics. These improved ocean colour products and relationships would lead to better estimation of primary production using bio-optical productivity models (Arrigo et al., 2008; Hirawake et al., 2011). However, due to the lack of contemporaneous *in situ* measurements in the SO, these particulate bio-optical relationships obtained from space have not been thoroughly evaluated and validated.

More observations are now available due to the BGC-Argo program, which deploys autonomous profiling floats worldwide, particularly in the SO, following the initial deployments by the Southern Ocean Carbon and Climate Observations and Modelling (SOCCOM) program (Sarmiento et al., 2023). To maximise the use of the BGC-Argo data, continuing efforts have been made to accurately convert chlorophyll fluorescence signals into chlorophyll *a* concentrations (Johnson et al., 2017; Roesler et al., 2017; Schallenberg et al., 2022). Particulate backscattering coefficients (b_{bp}) at 700 nm have been used to estimate POC in the SO by Johnson et al. (2017). In addition, Schallenberg et al. (2019) used 6 years of mooring data collected at the Southern Ocean Time Series (SOTS) site in the Subantarctic Zone south of Australia to estimate carbon-to-Chl ratios and interpret their seasonal dynamics. However, these particulate bio-optical relationships applied to float data in these studies were empirically developed based on limited concurrent measurements from hydrological casts on cruises. It is still unknown whether they are suitable for waters other than those where the relationships were developed.

In addition to pigment concentration (a desirable proxy for phytoplankton biomass) and the b_{bp}, hydrological casts during cruises can also provide data on mass concentrations (e.g., POC, particulate organic nitrogen (PON), macronutrients, and trace metal) and particle size distribution. These variables are essential for a better understanding of the particulate bio-optical properties and relationships in the SO. Based on ~ 280 samples collected during the Antarctic Circumpolar Expedition (ACE), Robinson et al. (2021) found that high-latitude SO phytoplankton have distinctive absorption properties compared to lower-latitude populations. However, other particulate bio-optical properties of the SO remain poorly observed and understood, leaving the question of whether they conform to or diverge from global relationships unanswered. Both the correct interpretation of satellite ocean colour observations and the appropriate parameterisation of bio-optical properties in biogeochemical models rely on this answer.

To address this gap, we collated field measurements from both hydrological casts and BGC-Argo floats to derive relationships among variables that are commonly used to describe the particulate pool, namely the particulate backscattering coefficient, b_{bp} (m^{-1}), the particulate absorption coefficient, a_p (m^{-1}), Chl (mg m^{-3}), POC (mg m^{-3}), and phytoplankton carbon (C_{phyto}, mg C m^{-3}). We specifically aim to elucidate large-scale distribution patterns of particle-related properties and evaluate the applicability of particulate bio-optical relationships developed for temperate oceanic waters to the SO.

2 Materials and methods

2.1 Datasets

The field data used in this study were acquired during the ACE aboard the RV Akademik Tryoshnikov during the austral summer from 20 December 2016 to 19 March 2017 (Walton and Thomas, 2018), and during the Southern Ocean Large Areal Carbon Export (SOLACE) research voyage aboard the RV Investigator (voyage IN2020_V08) from 05 December 2020 to 16 January 2021 (Figure 1). The ACE cruise travelled eastward around the Southern Ocean, starting from Cape Town, South Africa, to Hobart, Australia (leg 1), then proceeding via the Pacific Ocean to Punta Arenas, Chile (leg 2), and finally returning through the Atlantic Ocean back to Cape Town (leg 3). The SOLACE cruise investigated three sites: a subpolar site—SOTS (47°05′S, 141°22′E, Wynn-Edwards et al., 2019), and two polar possible phytoplankton bloom sites—Southern Site 1 (SS1, 55°49′S, 138°40′E) and Southern Site 2 (SS2, 57°54′S, 141°32′E), along with several stations during the transit (Figure 1, inset).

Measurements from both cruises and BGC-Argo floats were classified based on the seven bioregions defined by Ardyna et al. (2017) (Figure 2). This split aims to examine whether our dataset evenly samples various oceanographic regimes and to assess whether there are regional differences in the particulate bio-optical properties in addition to their large-scale patterns. The data from floats mostly fall into bioregions 3, 4, and 5, with only one-third belonging to the other bioregions. The distribution of cruise data is similar to that of float data, although high-latitude regions 6 and 7 are more prominently represented. Only average values from the top 10 m of the BGC-Argo data profiles are used in this work, combined with cruise data from underway sampling (depth ~5 m) and the top 10 m of data from CTD casts, as described in the following sections.

The BGC-Argo profiling floats (https://biogeochemical-argo.org) used in this study, equipped with CTD and bio-optical sensors, measured temperature, salinity, pressure, chlorophyll fluorescence, and volume scattering (used to derive backscattering coefficient). Figure 1 shows the geographical location of all profiles collected by 254 floats from January 2016 to June 2023. The data points are colour-coded based on the bioregions in which the floats operated, following the regionalisation outlined by Ardyna et al. (2017).

2.2 Phytoplankton pigments and particulate absorption

Phytoplankton pigment concentrations from ACE and SOLACE were determined using high-performance liquid chromatography (HPLC, see details in Ras et al. (2008); Antoine et al. (2020) and references therein). On both cruises, 2.2 L water samples were collected either 3 hourly from the underway seawater supply (sampling depth ~ 5 m) or from the shallowest depth of the

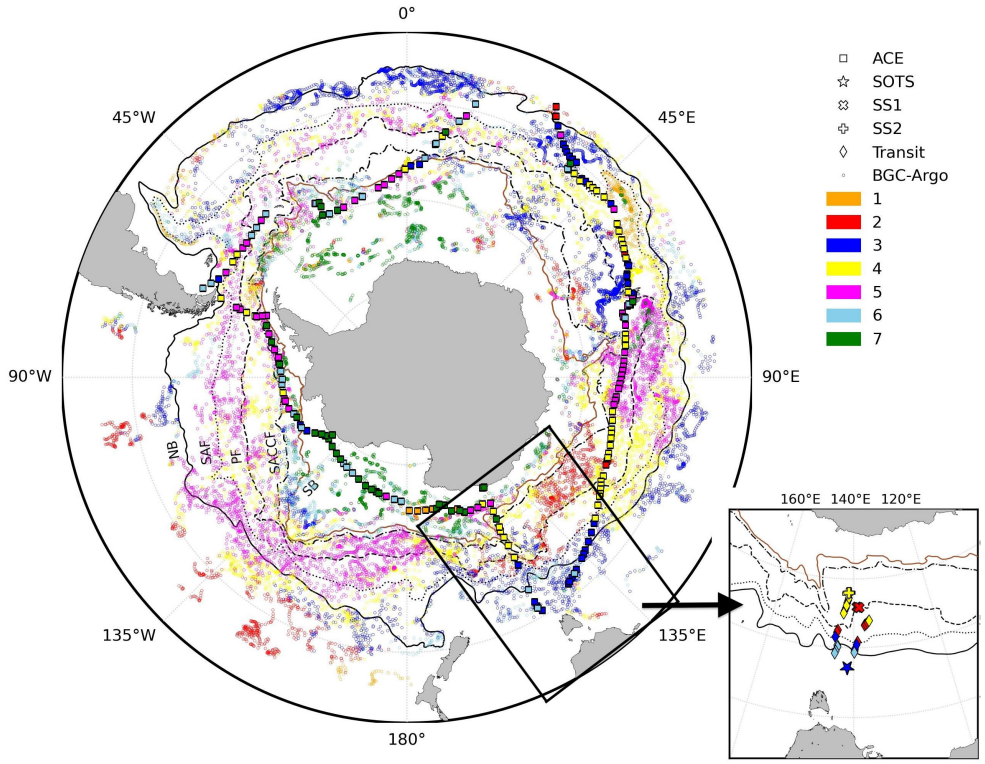

FIGURE 1
Sampling locations during ACE (squares) and SOLACE (SOTS, SS1, SS2, and transit sites, inset), as well as surface sampling points from BGC-Argo floats, colour-mapped according to the bioregions described in Ardyna et al. (2017). The Northern boundary (NB), Subantarctic Front (SF), Polar Front (PF), Southern Antarctic Circumpolar Current Front (SACCF), and Southern boundary (SB) from Park et al. (2019) are also displayed (black lines).

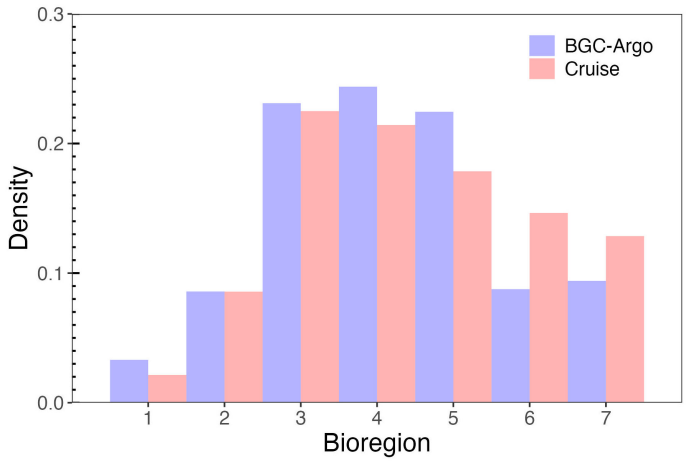

FIGURE 2
Distribution of cruise and float measurements among the seven bioregions defined by Ardyna et al. (2017).

conductivity, temperature, and depth (CTD) rosette casts (see Table 1 for a summary of the number of samples). Total chlorophyll *a* concentration was defined as the sum of mono- and divinyl chlorophyll *a* concentrations, chlorophyllide *a*, and the allomeric and epimeric forms of chlorophyll *a* (Hooker and Zibordi, 2005; Reynolds et al., 2016).

The pigments are used here to determine the relative contributions of micro- (f_{micro}, > 20 μm), nano- (f_{nano}, 2–20 μm), and picophytoplankton (f_{pico}, < 2 μm) to the total population, following Brewin et al. (2015).

For the BGC-Argo floats, the calibrated fluorescence profiles were adjusted for nonzero deep values (below 600 dbar) and corrected for spikes using a five-point median filter. Subsequently, they were divided by 3.79, as recommended by Schallenberg et al. (2022) for the SO. The surface Chl was obtained by averaging the values within the top 10 dbar.

A full description of the determination of the absorption coefficient of phytoplankton and non-algal particles (NAP) from the total particulate absorption coefficient can be found in Robinson et al. (2021), which is not repeated here.

2.3 Backscattering measurements

The particulate backscattering coefficient, $b_{bp}(\lambda)$ (m^{-1}), was determined on ACE and SOLACE using HOBI Labs HydroScat-6 sensors, which provide a measurement of the total spectral volume scattering function $\beta(\psi)$ (m^{-1} sr^{-1}) at an effective scattering angle $\psi = 140°$. The following equation (Maffione and Dana, 1997) was used to convert $\beta(140°, \lambda)$ to b_{bp} (λ),

$$b_{bp}(\lambda) = 2\pi\chi[\beta(140°, \lambda) - \beta_w(140°, \lambda)] \quad (1)$$

Where the subscripts p and w indicate the contributions from particles and seawater to scattering, respectively. χ is the coefficient of proportionality between β and b_b for particles, set to 1.13 for the HydroScat. Pure water values for $\beta_w(140°, \lambda)$ at given temperature and salinity were calculated following Zhang et al. (2009). Finally, vertical profile data of $b_{bp}(\lambda)$ were filtered to remove spikes and averaged into 0.5 m depth bins for analysis and correlation with discrete water samples. The Hydroscat channels were 420 nm, 488 nm, 550 nm, 620 nm, and 700 nm for ACE (the 442 nm channel failed), and 420 nm, 442 nm, 470 nm, 510 nm, 590 nm, and 700 nm for SOLACE. For ACE, only 13 b_{bp} spectra were obtained, primarily during leg 2 near the Antarctic continent.

To examine the wavelength dependency of particle backscattering, discrete spectral measurements were fitted to a power function of the following form:

$$b_{bp}(\lambda) = b_{bp}(\lambda_0)\left(\frac{\lambda}{\lambda_0}\right)^{\eta} \quad (2)$$

Where λ_0 represents a reference wavelength, and η denotes the dimensionless spectral slope of b_{bp}. Nonlinear least-squares fitting was applied to account for b_{bp} at all channels to derive η. Since the 442-nm spectral channel failed during the ACE cruise, this wavelength was excluded from the fitting of spectral relationships for the SOLACE cruise to ensure consistency between cruises.

Since our focus is on the total particle pool, we did not apply the nonzero deep value correction to the backscattering profile of BGC-Argo floats, as proposed by Uchida et al. (2019). This correction is meant to isolate the part of b_{bp} attributed to phytoplankton by removing the average of deep values (below 600 dbar), which are assumed to represent the NAP contribution. We applied a five-point median filter to remove spikes (Carranza et al., 2018; Mignot et al., 2018). Surface values were obtained by averaging the data within the top 10 dbar of the profile.

TABLE 1 Summary of the in situ dataset.

	Chl	$b_{bp}(\lambda)$	$a_p(\lambda)$	POC	PSD
ACE	221	13	274	355	264
SOLACE	31	3	31	3	3
BGC-Argo floats	21,872	21,872	–	–	–

2.4 Particulate organic carbon concentration

For the ACE dataset, the concentration of POC was obtained from the underway seawater supply every 3 h, as well as from several depths during the CTD rosette casts, and processed at the University of Cape Town (Fawcett and Forrer, 2020). Up to 2 L water samples were filtered through precombusted 25 mm GF/F filters. The filters were then dried at 40°C for 24 h, acidified to remove inorganic carbon, and stored until elemental analysis. Finally, POC for each sample was obtained by subtracting the average concentration of carbon in the dry blanks and was expressed in units of milligrammes per cubic metre. Samples outside the detection limits were eliminated. The same methodology was used for the SOLACE POC data, although it was processed at the University of Tasmania by Cathryn Wynn-Edwards.

2.5 Particle size distributions

The particle size distributions (PSD) determine their optical properties along with the particle composition. During ACE, PSD was measured with a Beckmann Coulter Counter Multisizer, which measures particle sizes by quantifying changes in electrical resistance produced by particles suspended in seawater as they pass through an aperture (Kinsman, 2018). In this study, 0.2 µm filtered seawater was used as the blank to detect particles in the range of 2–60 µm across 400 bins at each underway station. Twenty replicate measurements of 2 ml subsamples were made by the Counter for each sample and summed up to provide larger sample volumes, thereby improving statistical accuracy. Each discrete Coulter measurement included a set of values representing the particle concentrations (m^{-3}) within a size bin D, $N(D)$. The bin diameters were restricted to 2–30 µm, as no particles were observed in larger bins. Plots of particle concentration versus bin diameter were visually inspected, and samples with high noise levels or particle concentrations constrained to just a few bins were flagged as poor quality and removed (Robinson et al., 2021). Finally, 264 records of PSD were retained for further analysis.

During SOLACE, the PSD of large (> 100 µm) particles was measured using an Underwater Video Profiler 5 (UVP-5, Picheral et al., 2010) mounted on the rosette. Particle cross-sectional areas are quantified by assessing the contiguous pixels for a given image brightness level, which were then used to estimate the equivalent circular diameter. Finally, PSDs were determined for 24 bins, with centre bin sizes ranging from 115 to 23,300 µm. An upper limit of 2,315 µm was chosen to avoid regions of low particle counts and high statistical noise at large particle diameters. All data were binned vertically into 5-m intervals, and only surface values were used in this study.

The particle size distribution was fitted to a power law model (Bader, 1970; Jonasz and Fournier, 2011):

$$N(D) = N_0 \left(\frac{D}{D_0}\right)^{\zeta} \quad (3)$$

Where D_0 is a reference diameter, N_0 is the particle number at D_0, and ζ is the dimensionless slope of the distribution. For the Coulter measurements, these metrics were calculated to characterize the samples and were computed over the size range of 4–20 µm. Since ζ is very sensitive to the range of effective diameters used and can be biased when an abundant phytoplankton cell size is present, leading to a bump on the PSD, we visually inspected the spectra and removed 15 spectra where clear bumps were present to avoid these cases.

2.6 Phytoplankton carbon estimations

C_{phyto} is a key parameter in estimating primary production using various models (Sathyendranath et al., 2007). It also allows an understanding of phytoplankton physiology, as reflected in variations of cellular chlorophyll-to-carbon ratios generated by changes in light, temperature, and nutrients (Behrenfeld et al., 2005). However, C_{phyto} is difficult to distinguish experimentally *in situ* or in laboratory studies from the total carbon included in phytoplankton plus zooplankton, detritus, and bacteria. Consequently, direct C_{phyto} estimations are scarce, and essentially proxy measurements have been used to quantify it, such as Chl, cell biovolume, POC, and b_{bp}.

Here, in the absence of direct C_{phyto} measurements, it was estimated using either the POC vs. Chl relationship or from b_{bp}. The former approach assumes that at any given Chl, the lowest POC observed represents the phytoplankton fraction, C_{phyto} (Sathyendranath et al., 2009). In this approach, a 1% quantile regression is applied to the fit between POC and Chl to obtain C_{phyto}, hereafter denoted as C_{phyto}-S09. Since there will always be some contribution to POC from material other than phytoplankton, such as heterotrophs and detritus, this C_{phyto} estimate likely represents an upper limit for a given Chl. In addition, this approach does not allow for scenarios where C_{phyto} increases or decreases without a corresponding change in Chl (Thomalla et al., 2017). However, it is unlikely to be influenced by phenomena such as coccolith blooms or bubbles, which can significantly increase backscattering or the attenuation coefficient without increasing Chl.

Backscattering-based approaches allow C_{phyto} to vary independently of Chl, making them less susceptible to the package effect or photoacclimation. As a result, they are able to detect the high temporal variability in Chl:C_{phyto} ratios. These methods assume C_{phyto} is linearly related to b_{bp}. Behrenfeld et al. (2005) established such a relationship by fitting satellite-derived b_{bp} (440) to which a background value of 3.5×10^{-4} m^{-1} is subtracted to laboratory C_{phyto} values:

$$C_{phyto} = 13{,}000 \times (b_{bp}(440) - 3.5 \times 10^{-4}) \quad (4)$$

which is denoted as C_{phyto}-B05 hereafter. The subtraction of the background value accounts for the portion of backscattering attributed to a background of NAP that does not covary with phytoplankton.

Based on direct measurements of both C_{phyto} and b_{bp} in the Atlantic Ocean, Martinez-Vicente et al. (2013) found a significant linear relationship between C_{phyto} and b_{bp}(470)

(denoted as C_{phyto}-M13):

$$C_{phyto} = 30{,}100 \times (b_{bp}(470) - 7.6 \times 10^{-4}) \quad (5)$$

This linear regression was initially limited to b_{bp} (470) < 0.003 m^{-1} or Chl < 0.4 mg m^{-3}; however, in this study, we extended it for the larger Chl range as well.

Using data from the Equatorial Pacific Ocean and from the 22nd Atlantic Meridional Transect cruise, Graff et al. (2015) established yet another relationship:

$$C_{phyto} = 12{,}128 \times b_{bp}(470) + 0.59 \quad (6)$$

Hereafter denoted as C_{phyto}-G15.

Note that, for backscatter measurements lacking a 440- or 470-nm channel, the values at 700 nm were converted to these other wavelengths using Equation 2, with η equal to 1.08 (mean of the measured values).

3 Results and discussions

3.1 General latitudinal distribution of properties

The latitudinal distribution of average values of major environment parameters and inherent optical properties (IOPs) is presented in Figure 3. These values are calculated from all data found in 2° latitude bands centred on latitudes from 40°S to 74°S. Hereafter, Chl and b_{bp} are measured both through ship-based hydrographic casts and BGC-Argo floats are denoted separately as Chl-*Cruise* and Chl-*Float* (and b_{bp}-*Cruise* and b_{bp}-*Float*).

Temperature decreases toward the south (Figure 3A), from about 15°C at 40°S to – 1°C close to the Antarctic continent. Salinity also shows a general decreasing trend toward the south (Figure 3B), with two relative maxima observed around 65°S and near the continent.

Minima of Chl-*Cruise* are found around 60°S~68°S and maxima around 45°S and 72°S (Figure 3C). The Chl-*Cruise* and Chl-*Float* are quite consistent, with the differences mainly due to the uneven cruise sampling. In the 41°S~45°S latitudinal belt, Chl-*Cruise* measurements were constrained in the area south of the African continent and are higher than Chl-*Float*. In the 59°S to 67°S latitudinal belt, Chl-*Cruise* was at the lowest level (< 0.2 mg m^{-3}) at the Drake Passage and the Dumont d'Urville Sea. As for the 69° S~76°S latitudinal belt, Chl-*Float* measurements are higher than Chl-*Cruise* and have larger variance because they were collected in more varied environments. Among the SOLACE data, Chl-*Cruise* is the highest at SOTS with a mean value of 0.64 mg m^{-3}, followed by SS2 (0.31 mg m^{-3}) and SS1 (0.15 mg m^{-3}).

The latitudinal distribution of a_{ph}(442) (Figure 3D) reflects that of Chl-*Cruise*, yet shows a smaller relative increase toward high latitudes, leading to a decrease of the chlorophyll-specific absorption coefficient at 442 nm, a^{*}_{ph}(442) (Figure 3E).

The fraction of larger phytoplankton, f_{micro}, increases from about 0.3 to 0.9 toward the south (Figure 3F), which is consistent with the findings by Robinson et al. (2021).

Generally, b_{bp} (700) (Figure 3G) is quite stable in the 40 to 60°S belt, with a mean value of ~ 0.0012 m^{-1}. South of 60°S, the mean values and associated variance both increase. The 16 b_{bp}-*Cruise* all fall within the range of the b_{bp}-*Float* values. Due to the very limited b_{bp} measurements on cruises, they were excluded from further analyses with respect to the large-scale latitudinal analyses. The mean b_{bp}:Chl ratios across latitudes (Figure 3H) fluctuate between 0.005 and 0.008 m^2 mg^{-1}.

The POC (Figure 3I) varies between 30 and 200 mg m^{-3}, with minimum values around 60°S and an average value of 105 mg m^{-3} across the dataset. The POC:Chl ratio (Figure 3J) varies over one order of magnitude, from 100 to 1,000, and shows relative maxima around 54°S and 64°S, with a regular decrease for latitude south of about 64°S.

It is worth noting that BGC-Argo data from all seasons have been pooled together here, whereas the cruise data are for the summer months only (December to February, plus early March for ACE). If Figure 3 was to include BGC-Argo data for only the 3 summer months, the only two notable differences would be the slightly higher b_{bp}(700) values (0.002 instead of 0.0015 m^{-1} on average for latitudes above 70°S) and, similarly, the slightly higher Chl for latitudes above 60°S (with an average of approximately 0.4 instead of 0.25 mg m^{-3}). The discrepancy between Chl-*Cruise* and Chl-*Float* would be reinforced in the 60°S–68°S band, primarily due to the ship sampling being restricted to the Drake Passage and Dumont d'Urville Sea.

When the zonal averages displayed in Figure 3 are restricted to the Atlantic, Indian, and Pacific sectors, the latter displays the lowest Chl (average 0.2 mg m^{-3}). In contrast, the subtropical latitudes of the Indian Ocean are saltier (salinity ~ 35 psu), warmer (SST up to 17°C), and have the largest POC concentrations (around 100 mg m^{-3}). No other major differences are observed among the three sectors and between the results for each sector and those for the entire SO.

3.2 Bio-optical relationships

The various bio-optical relationships we have explored are illustrated in Figure 4. The ratio of NAP to phytoplankton absorption, a_{NAP}: a_{ph} (Figure 4A), shows an upward tail in low Chl waters (Chl < 0.2 mg m^{-3}), with values larger than 1 and as large as 10. For larger Chl values (> 0.2 mg m^{-3}), the ratio slowly decreases as Chl increases. This result not only suggests a high contribution of NAP, such as heterotrophs and detritus, to the particle pool in clear waters of the SO, but also that this contribution is highly variable.

This large contribution of NAP to the particle pool in the SO seems corroborated by the POC vs. Chl relationship (Figure 4B). Here, Chl-*Cruise* varies over nearly three orders of magnitude, and POC over two, and their relationship shows the generally expected increasing trend but only for Chl > 0.2 mg m^{-3}. Below this concentration, POC fluctuates around 80 mg m^{-3}, independent of Chl levels, again suggesting that NAP significantly contributes to POC in the clear waters of the SO.

10.3389/fmars.2024.1466037

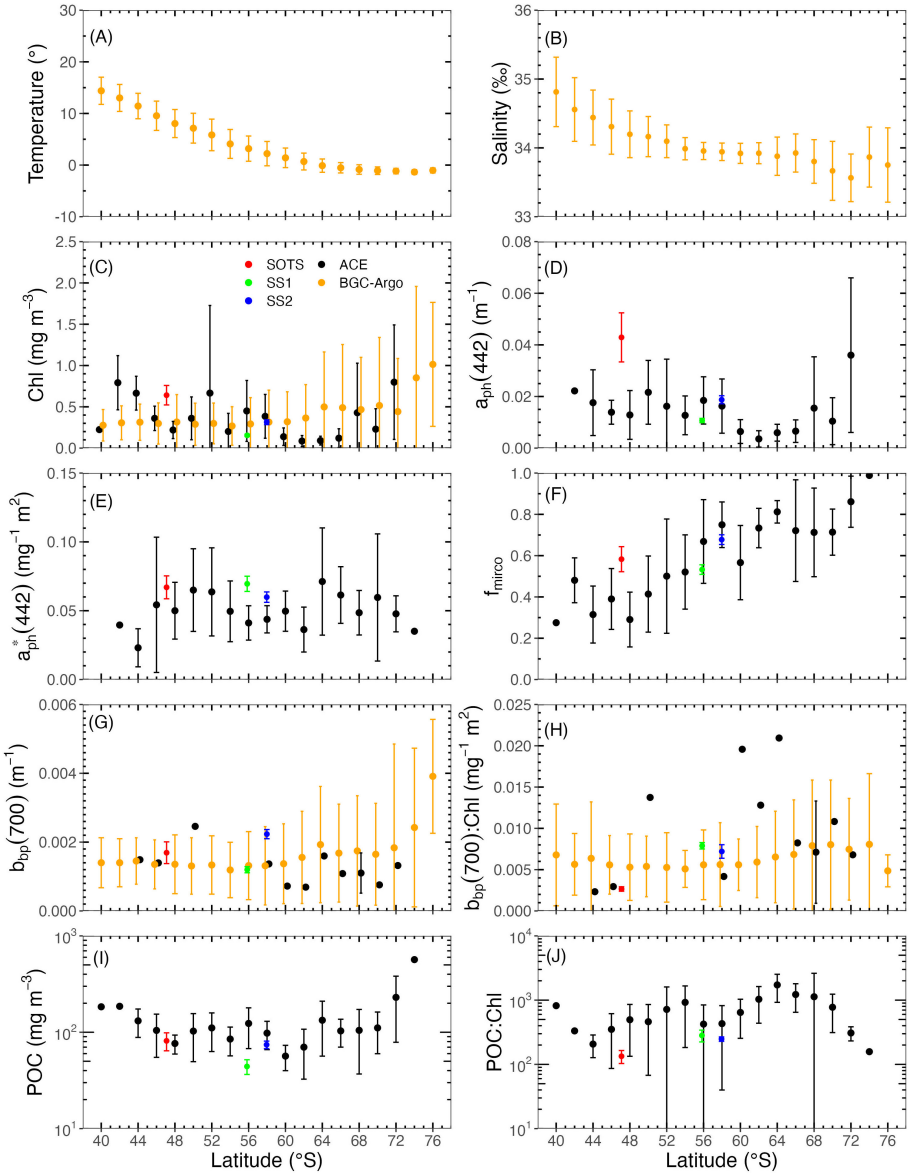

FIGURE 3
Latitudinal distribution of **(A)** temperature, **(B)** salinity, **(C)** Chl, **(D)** $a_{ph}(442)$, **(E)** $a^*_{ph}(442)$, **(F)** f_{micro}, **(G)** $b_{bp}(700)$, **(H)** $b_{bp}(700)$ to Chl ratio, **(I)** POC, and **(J)** POC to Chl ratio. Black symbols represent measurements made from hydrographic casts on ships, while orange symbols refer to BGC-Argo float measurements. The red, blue, and green dots refer to the SOTS, SS1, and SS2 sites, respectively. Data were grouped into 2° latitude intervals, within which the mean values and standard deviations were calculated.

The POC vs. Chl relationship is generally expressed through a linear fit on log-transformed data. For instance, Sathyendranath et al. (2009) found such a linear relationship (r^2 = 0.58) using data from the equatorial Pacific and Atlantic Oceans, denoted POC-S09 hereafter (solid purple line in Figure 4B). In our study, a linear regression in log space is not appropriate to describe the POC vs. Chl relationship because of the relatively constant POC in waters where Chl is less than 0.2 mg m^{-3}, attributed to the contribution of NAP to POC. Therefore, we added a constant background POC in our linear regression. When a linear fit without constant background value is applied to data for Chl > 0.2 mg m^{-3} only, the obtained POC vs. Chl relationship shows no significant difference with POC-S09.

We also applied 1% quantile regression on the data where Chl > 0.2 mg m^{-3} to derive C_{phyto}, following the approach of Sathyendranath et al. (2009), resulting in a remarkably similar relationship (dashed and solid purple lines in Figure 4B). By converting b_{bp}-*Float* to C_{phyto} according to Behrenfeld et al. (2005); Martinez-Vicente et al. (2013), and Graff et al. (2015), C_{phyto} vs. Chl can be obtained as well, denoted as B05, M13 and G15, respectively. Their comparison with S09 is illustrated in Figure 4C. The slope of M13 is significantly higher than the others, resulting in a difference up to 160 mg m^{-3} in C_{phyto} at Chl = 3 mg m^{-3}. B05 and G15 have similar intercepts, although the slope of B05 is slightly higher. Their largest difference is about 50 mg m^{-3} in C_{phyto} at Chl = 6 mg m^{-3}. S09 generally derives higher C_{phyto} per Chl, while G15 intersects with B05

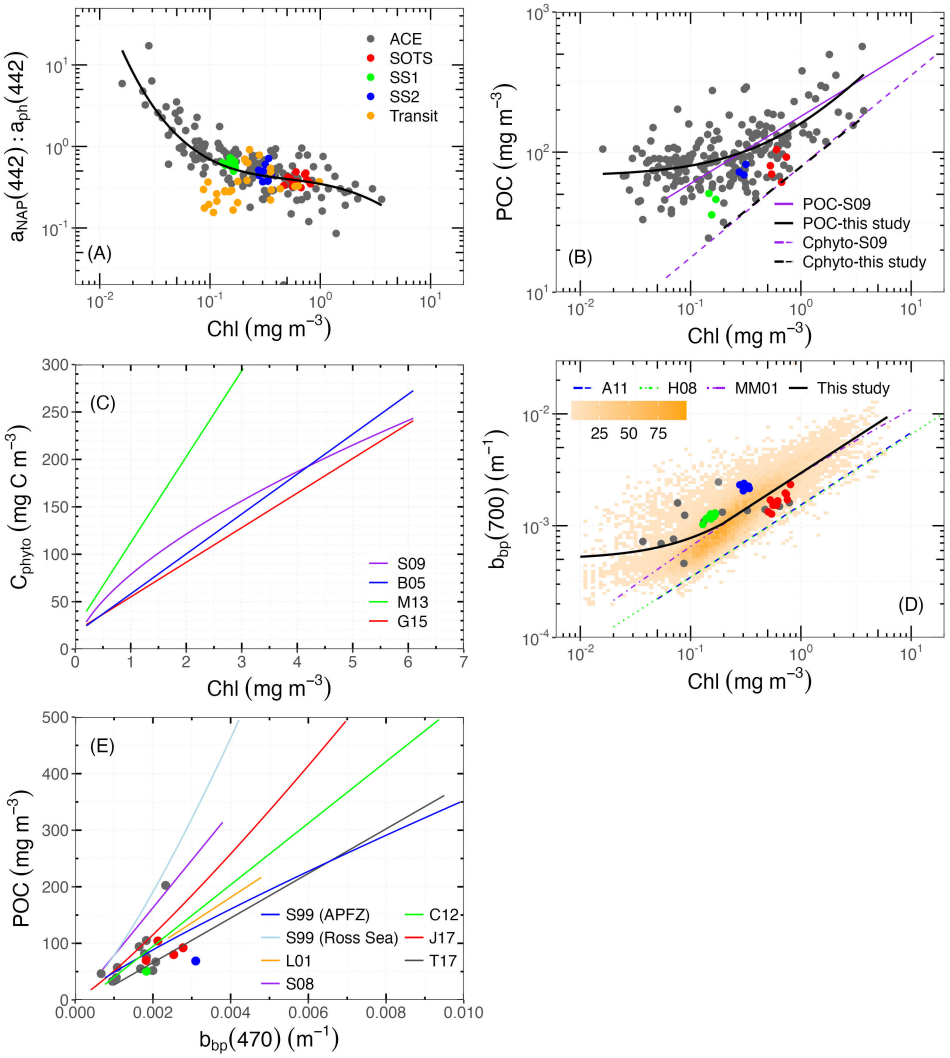

FIGURE 4
Bio-optical relationships. **(A)** a_{NAP}:a_{ph} ratio at 442 nm vs. Chl. The black solid line represents the fourth-degree polynomial regression in log space for our dataset, $y = -0.26 - 3.0x + 1.36x^2 - 0.90x^3 + 0.08x^4$ ($y = \log_{10}(a_{NAP}(442)/a_{ph}(442))$, $x = \log_{10}$Chl, $n = 201$, $r^2 = 0.57$). **(B)** POC vs. Chl. The black solid curve represents POC = 67.4 + 93.3 Chl$^{0.87}$ ($n = 229$, $r^2 = 0.42$). The dashed black line represents the 1% quantile regression on the same data, representing the relationship between C_{phyto} and Chl (C_{phyto} = 78.5 Chl$^{0.63}$), following Sathyendranath et al. (2009). The purple solid and dashed lines refer to the POC vs. Chl and C_{phyto} vs. Chl relationships from Sathyendranath et al. (2009), respectively. **(C)** C_{phyto} vs. Chl. See Section 2.6 for S09, B05, M13, and G15. **(D)** $b_{bp}(700)$ vs. Chl. The background orange symbols refer to the density of float measurements. The solid black line represents the regression line between $b_{bp}(700)$ and Chl, using both ship and float data from this study: $b_{bp}(700) = 0.0005 + 0.0028$ Chl (Chl $\leq$ 0.2 mg m^{-3}); $b_{bp}(700) = 0.0031$ Chl$^{0.67}$ (Chl > 0.2 mg m^{-3}). The blue, green, and purple lines refer to the relationships from Antoine et al. (2011) in the Northwestern Mediterranean Sea and Santa Barbara Channel, Huot et al. (2008) in the Eastern South Pacific Ocean, and Morel and Maritorena (2001) for global oceanic waters, respectively. **(E)** POC vs. $b_{bp}(470)$. S99, L01, S08, C12, J17, and T17 refer to the relationships from Stramski et al. (1999) in the Antarctic Polar Front Zone (APFZ) and the Ross Sea, Loisel et al. (2001) in the Mediterranean Sea, Stramski et al. (2008) in the Pacific and Atlantic Oceans, Cetinić et al. (2012) in the North Atlantic Ocean, Johnson et al. (2017) in the SO, and Thomalla et al. (2017) in the South Atlantic and SO, respectively. Note that for models without b_{bp} at 470 nm, values were propagated from other available bands according to Equation 2 using $\eta = 1.08$.

at Chl = 4.3 mg m^{-3}, with their differences in C_{phyto} remaining within 50 mg m^{-3} across all Chl ranges.

B05 and M13 assume a constant background b_{bp} due to NAP (denoted bbp-NAP) that does not covary with phytoplankton. However, Bellacicco et al. (2016) found that b_{bp}-NAP varies both seasonally and regionally by more than one order of magnitude, which might result in significant errors in the C_{phyto} estimates. G15 is the only one using analytical field-measured C_{phyto}, which has been found to have a significant correlation with b_{bp} in the Equatorial Pacific Ocean and Atlantic Ocean.

None of these methods (either Chl or b_{bp}-based) have been derived using data collected in the SO, so their applicability here cannot be ascertained. Their consistent C_{phyto} prediction is however encouraging. It is still worth noting that the aforementioned approaches do not seem applicable to waters with Chl < 0.2 mg m^{-3}, due to the high NAP contribution to the particle pool. The substantial contribution of NAP to POC and b_{bp} further complicates the accurate estimation of C_{phyto} in such waters. Therefore, sufficient concurrent measurements of phytoplankton community composition and their specific chlorophyll and carbon

content are needed to evaluate and validate optical methods of determining C_{phyto} concentrations, and then to assess Chl: C_{phyto} ratios for better understanding phytoplankton physiology under environmental forcing.

The b_{bp}-*Cruise* and b_{bp}-*Float* data are displayed as a function of Chl in Figure 4D. The former varies between 0.0004 and 0.004 m^{-1} in the combined ACE and SOLACE dataset, and all fall within the larger range (0.0002~0.1 m^{-1}) measured by floats over the entire SO. Values obtained during SOLACE were generally higher than those observed during ACE leg 2 near the Antarctic continent. The highest values were obtained at SS2 with the smallest variation, followed by those at SOTS and SS1. The spectral slope of $b_{bp}(\lambda)$, calculated using all available wavebands, fluctuates from 0.5 to 1.6, with a mean value of 1.08. The b_{bp}-*Float* values generally increase with Chl, although they remain relatively constant in the low Chl range (again, Chl < 0.2 mg m^{-3}). For Chl > 0.2 mg m^{-3}, b_{bp} covaries with Chl, which is consistent with previous observations (Antoine et al., 2011; Bellacicco et al., 2019). Therefore, we here combined a linear regression for Chl < 0.2 mg m^{-3} with a power law for Chl > 0.2 mg m^{-3} to fit the data (solid black curve in Figure 4D).

For comparison, other relationships obtained from *in situ* data collected in the Northwestern Mediterranean Sea and Santa Barbara Channel by Antoine et al. (2011) (denoted A11) and in the Eastern South Pacific Ocean by Huot et al. (2008) (denoted M08) are also shown. For A11, their $b_{bp}(560)$ was converted to $b_{bp}(700)$ according to Equation 2. The $b_{bp}(700)$ vs. Chl relationship from Morel and Maritorena (2001) (denoted MM01) developed for the oceanic case I waters is shown as well. Generally, the $b_{bp}(700)$ of MM01 is significantly higher than H08 and A11 across the Chl range, which might be due to the difference in study regions. For Chl > 0.2 mg m^{-3}, our fit generally coincides with MM01, but with a slightly larger slope. For Chl < 0.2 mg m^{-3}, $b_{bp}(700)$ is higher than predicted by MM01, with differences that can reach up to one order of magnitude. The high contribution of NAP is likely responsible for these larger b_{bp} values in clear waters as compared to what global models predict from Chl. Such relative constant b_{bp} is likely a consequence of the combination of photoacclimation and the high proportion of NAP. The former is typical for polar waters, where Chl variation is driven by photoacclimation to low light and thus uncoupled with biomass, leading to an increase of Chl without a corresponding increase in b_{bp} (Behrenfeld et al., 2005; Brewin et al., 2012; Bellacicco et al., 2019).

It is also worth noting that we did not find significant differences among b_{bp}-*Float* vs. Chl-*Float* relationships as separately derived for each Ardyna's bioregions.

The ACE and SOLACE datasets have only 16 concurrent measurements of POC and $b_{bp}(470)$. They are shown in Figure 4E on top of relationships obtained from both temperate oceans and subregion of the SO (see figure caption for details). There is a large spread of POC vs. $b_{bp}(470)$ relationships across different regions. The highest POC: $b_{bp}(470)$ statistical mean ratio is noticed in the Ross Sea, while the lowest is also found in the SO from 20°W ~ 20°E by Thomalla et al. (2017). In addition, their difference in POC is about 350 mg m^{-3} at $b_{bp}(470)$ = 0.004 m^{-1} and continues to increase as b_{bp} increases. Thus, there is no clear POC vs. b_{bp} relationship in the SO, especially for high-scattering waters. This lack of correlation is due to the contributions of both POC and particulate inorganic carbon (PIC) to backscattering.

It appears that in the SO, we cannot use a single linear regression to describe the relationships of bio-optical properties and chlorophyll over the full concentration range. For Chl < 0.2 mg m^{-3}, the large NAP contribution tends to mask any possible phytoplankton-related changes in bio-optical properties.

3.3 Particle size distributions

PSD of surface waters measured by the Coulter Counter and UVP-5 are illustrated in Figure 5. Particle concentrations (m^{-3} μm^{-1}) decrease when the equivalent spherical diameter increases and generally follow a Junge-type size distribution. This is expected, yet exceptions occur, with peaks appearing at certain diameters, e.g., 10 µm, which may indicate phytoplankton blooms dominated by a particular size group. Although the Coulter and UVP-5 use different approaches to determine particle size, cross-sectional area for the UVP-5, and particle volume for the Coulter

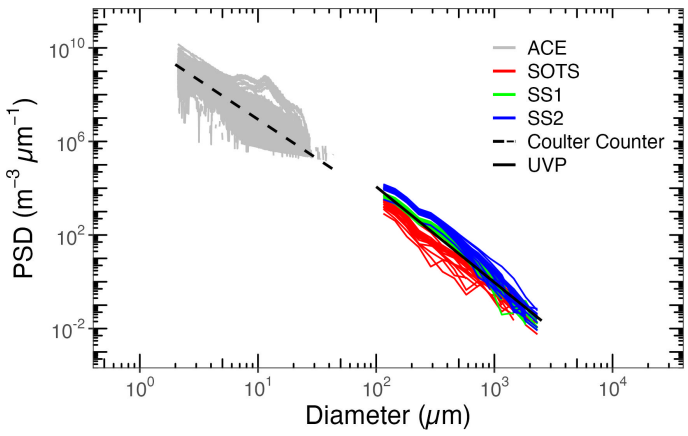

FIGURE 5
Particle size distributions derived from Coulter Counter and UVP-5.

10.3389/fmars.2024.1466037

Counter, the slopes determined over different size ranges are quite similar (a mean value of 3.99 for Coulter Counter data and 4.29 for UVP-5 data). Among the SOLACE data, the number of particles is overall larger at SS1 and SS2 than at SOTS, although the latter displays a larger Chl. This observation of more large particles (UVP-5 data start at 100 μm) at the two clearer southern sites seems consistent with the larger NAP contribution already identified for the domain of smaller particles.

PSD slopes (ζ, unitless) are displayed as a function of Chl, colour-mapped as a function of the fraction of microphytoplankton (f_{micro}) derived according to Brewin et al. (2015) (Figure 6). The slope ζ varies between 3 and 5. A somewhat decreasing trend can be discerned for Chl > 0.2 mg m^{-3}, similar to what Buonassissi and Dierssen (2010) have found in temperate regions, yet there is no significant relationship when Chl appears below 0.2 mg m^{-3}, suggesting the particle distribution is heterogenous within the SO. In addition, we did not notice a clear impact of f_{micro} on ζ. The expectation would be that populations dominated by larger cells would have a lower ζ, which is not clearly observed here.

3.4 Implications for ocean colour remote sensing

The absorption of NAP follows an exponential decay from the blue to the red parts of the spectrum. In the clear waters we have analysed here (Chl < 0.2 mg m^{-3}), the large NAP contribution leads to significant non-chlorophyll absorption in the blue part of the

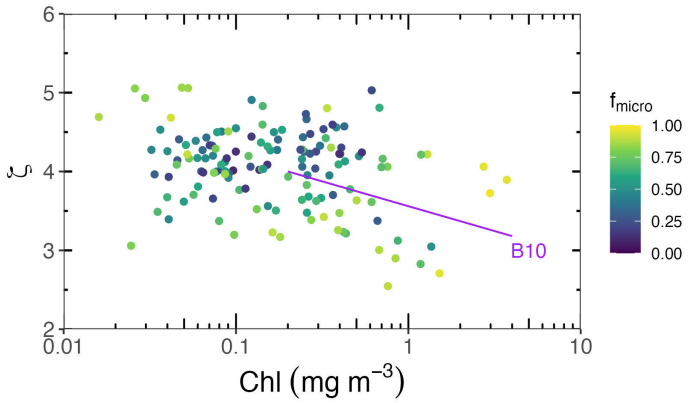

FIGURE 6
PSD slope ζ vs. Chl relationship. The dots are colour-mapped as a function of the fraction of micro-phytoplankton derived from Brewin et al. (2015). The purple line represents the relationship obtained by Buonassissi and Dierssen (2010) in the North Atlantic, where $\zeta = -0.63 \log_{10}\text{Chl} + 3.56$, $n = 25$, $r^2 = 0.45$.

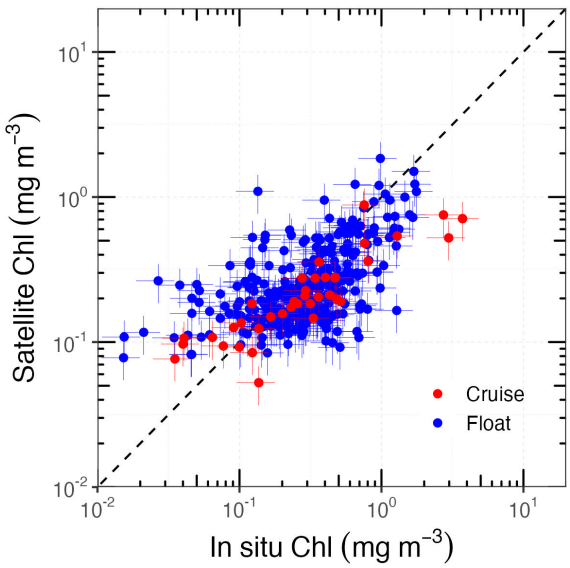

FIGURE 7
Comparisons between in situ and satellite-derived Chl. The black dashed line represents the 1:1 relationship. Error bars indicate the typical 30% uncertainty for both the HPLC- and satellite-derived Chl.

spectrum ($\lambda < \sim 500$ nm). A likely consequence is a lower blue-to-green remote-sensing reflectance band ratio than would otherwise exist for the same Chl concentration but with a lower NAP contribution. This would result in a significant overestimation of Chl when using global empirical ocean colour algorithms to derive Chl from the reflectance ratio, as the NAP absorption would be wrongly interpreted as phytoplankton absorption.

To verify this, we compared *in situ* Chl from both cruise and float measurements with satellite-derived Chl estimates. For this purpose, we used the Moderate Resolution Imaging Spectroradiometer (MODIS) L3b binned chlorophyll products, which use a sinusoidal projection so that each grid cell covers the same area, regardless of latitude. For each *in situ* measurement covered by a product, a 3 × 3 window centred on the *in situ* location was extracted. In total, we found 311 *in situ* and satellite-derived Chl matchups, which are displayed in Figure 7.

Previous similar matchup studies generally reported an underestimation of Chl by satellite products in the SO (Garcia et al., 2005; Marrari et al., 2006; Kahru and Mitchell, 2010; Szeto et al., 2011; Johnson et al., 2013; Jena, 2017; Pereira and Garcia, 2018; Moutier et al., 2019). This is confirmed here, but only for Chl > 0.2 mg m^{-3}. For lower values, we conversely observe an overestimation. This is consistent with the excess NAP absorption reported here. It cannot be ruled out, however, that larger absorption by coloured dissolved organic matter (CDOM) would also contribute to this overestimation of Chl (Morel and Gentili, 2009). The absence of reflectance measurements from the ACE and SOLACE voyages did not allow these hypotheses to be further tested here.

4 Conclusions

By combining ship-based measurements from the ACE and SOLACE research voyages and profiling-float-based measurements from over 20,000 profiles collected by the BGC-Argo network, we were able to analyse the general latitudinal distribution patterns of particle-related bio-optical and biogeochemical variables, as well as the associated bio-optical relationships.

At latitudes beyond 60°S, Chl, a_{ph}, b_{bp}, POC, and f_{micro} increase toward the Antarctic continent. In parallel, the chlorophyll-normalised values of a_{ph} and POC decrease, while the chlorophyll-specific b_{bp} remains stable across latitudes.

The absorption data showed a high proportion of NAP (a_{NAP}: a_{ph} up to 10) in the clear waters (Chl < 0.2 mg m^{-3}) of the SO. This substantial NAP contribution leads to higher POC and b_{bp} values, making particulate bio-optical properties significantly different from what is expected for temperate areas. In contrast, this divergence is not evident in waters with Chl > 0.2 mg m^{-3}. Therefore, using bio-optical relationships developed in temperate waters to study the SO is probably acceptable outside the domain of low Chl. The specific relationships we propose here (Figure 4) are presumably better adapted to the SO. Nonetheless, caution is warranted, as even minor alterations in these relationships can result in notable absolute differences due to the substantial variability present.

The implication for satellite ocean colour applications seems to be an overestimation of Chl in clear waters when using standard algorithms (again, in areas with Chl levels below 0.2 mg m^{-3}). Deriving better SO-adapted Chl retrieval algorithms that account for this peculiarity would, however, require more comprehensive datasets of bio-optical properties and radiometry measurements, which still do not exist at the required scale. This is definitely where more effort should be directed if we are to expect significant improvements in our ability to monitor SO ecosystems from space.

Data availability statement

Publicly available datasets were analyzed in this study. This data can be found here: BGC-Argo float data is available at https://biogeochemical-argo.org. Data collected during cruises is available at https://zenodo.org/records/3993096, https://doi.org/10.5281/zenodo.3816726, https://doi.org/10.5281/zenodo.3660852, https://doi.org/10.5281/zenodo.3706710.

Author contributions

JL: Conceptualization, Data curation, Formal analysis, Investigation, Methodology, Software, Validation, Visualization, Writing – original draft, Writing – review & editing. DA: Conceptualization, Data curation, Funding acquisition, Resources, Supervision, Writing – review & editing. YH: Conceptualization, Methodology, Supervision, Visualization, Writing – review & editing.

Funding

The author(s) declare financial support was received for the research, authorship, and/or publication of this article. JL was supported by the Australian Research Council Special Research Initiative, Australian Centre for Excellence in Antarctic Science (ACEAS; Project Number SR200100008). ACE was funded by Ferring Pharmaceuticals with additional support from the Swiss Polar Institute. Funding from the Australian Research Council Discovery Program (DP160103387) contributed to the exploitation of ACE data.

Acknowledgments

We would like to thank all members of the ACE Project, including Charlotte Robinson, William Moutier, David Berliner, Alexandra Olivier, and Hazel Little, as well as staff from the Swiss Polar Institute and the crew from the RV Akademik Trynoshnikov. SOLACE received support from the Australian Government through ship time at the Marine National Facility (MNF; R/V Investigator).

We thank the scientific staff and crew of the R/V Investigator for facilitating work at the three SOLACE sites in the Southern Ocean.

Conflict of interest

The authors declare that the research was conducted in the absence of any commercial or financial relationships that could be construed as a potential conflict of interest.

Publisher's note

References

Allison, D. B., Stramski, D., and Mitchell, B. G. (2010a). Empirical ocean color algorithms for estimating particulate organic carbon in the Southern Ocean. *J. Geophysical Research: Oceans* 115. doi: 10.1029/2009JC006040

Allison, D. B., Stramski, D., and Mitchell, B. G. (2010b). Seasonal and interannual variability of particulate organic carbon within the Southern Ocean from satellite ocean color observations. *J. Geophysical Research: Oceans* 115. doi: 10.1029/2009JC005347

Antoine, D., Siegel, D. A., Kostadinov, T., Maritorena, S., Nelson, N. B., Gentili, B., et al. (2011). Variability in optical particle backscattering in contrasting bio-optical oceanic regimes. *Limnology Oceanography* 56, 955–973. doi: 10.4319/lo.2011.56.3.0955

Antoine, D., Thomalla, S., Berliner, D., Little, H., Moutier, W., Olivier-Morgan, A., et al. (2020). *Phytoplankton pigment concentrations of seawater sampled during the Antarctic Circumnavigation Expedition (ACE) during the Austral Summer of 2016/2017*. doi: 10.5281/zenodo.3816726

Ardyna, M., Claustre, H., Sallée, J.-B., D'Ovidio, F., Gentili, B., van Dijken, G., et al. (2017). Delineating environmental control of phytoplankton biomass and phenology in the Southern Ocean. *Geophysical Res. Lett.* 44, 5016–5024. doi: 10.1002/2016GL072428

Arrigo, K. R., van Dijken, G. L., and Bushinsky, S. (2008). Primary production in the southern ocean 1997–2006. *J. Geophysical Research: Oceans* 113. doi: 10.1029/2007JC004551

Bader, H. (1970). The hyperbolic distribution of particle sizes. *J. Geophysical Res.* 75, 2822–2830. doi: 10.1029/JC075i015p02822

Behrenfeld, M. J., Boss, E., Siegel, D. A., and Shea, D. M. (2005). Carbon-based ocean productivity and phytoplankton physiology from space. *Global Biogeochem. Cycles.* 19. doi: 10.1029/2004GB002299

Belcher, A., Iversen, M., Manno, C., Henson, S. A., Tarling, G. A., and Sanders, R. (2016). The role of particle associated microbes in remineralization of fecal pellets in the upper mesopelagic of the Scotia Sea, Antarctica. *Limnology Oceanography* 61, 1049–1064. doi: 10.1002/lno.10269

Bellacicco, M., Cornec, M., Organelli, E., Brewin, R. J. W., Neukermans, G., Volpe, G., et al. (2019). Global variability of optical backscattering by non-algal particles from a biogeochemical-argo data set. *Geophysical Res. Lett.* 46, 9767–9776. doi: 10.1029/2019GL084078

Bellacicco, M., Volpe, G., Colella, S., Pitarch, J., and Santoleri, R. (2016). Influence of photoacclimation on the phytoplankton seasonal cycle in the Mediterranean Sea as seen by satellite. *Remote Sens. Environ.* 184, 595–604. doi: 10.1016/j.rse.2016.08.004

Boyd, P. W., Claustre, H., Levy, M., Siegel, D. A., and Weber, T. (2019). Multi-faceted particle pumps drive carbon sequestration in the ocean. *Nature* 568, 327–335. doi: 10.1038/s41586-019-1098-2

Boyd, P. W., McDonnell, A., Valdez, J., LeFevre, D., and Gall, M. P. (2015). RESPIRE: An in situ particle interceptor to conduct particle remineralization and microbial dynamics studies in the oceans' Twilight Zone. *Limnology Oceanography: Methods* 13, 494–508. doi: 10.1002/lom3.10043

Brewin, R. J. W., Dall'Olmo, G., Sathyendranath, S., and Hardman-Mountford, N. J. (2012). Particle backscattering as a function of chlorophyll and phytoplankton size structure in the open-ocean. *Opt. Express* 20, 17632–17652. doi: 10.1364/OE.20.017632

Brewin, R. J. W., Sathyendranath, S., Jackson, T., Barlow, R., Brotas, V., Airs, R., et al. (2015). Influence of light in the mixed-layer on the parameters of a three-component model of phytoplankton size class. *Remote Sens. Environ.* 168, 437–450. doi: 10.1016/j.rse.2015.07.004

Briggs, N., Dall'Olmo, G., and Claustre, H. (2020). Major role of particle fragmentation in regulating biological sequestration of CO_2 by the oceans. *Science* 367, 791–793. doi: 10.1126/science.aay1790

Buesseler, K. O., Lamborg, C. H., Boyd, P. W., Lam, P. J., Trull, T. W., Bidigare, R. R., et al. (2007). Revisiting carbon flux through the ocean's twilight zone. *Science* 316, 567–570. doi: 10.1126/science.1137959

Buonassissi, C. J., and Dierssen, H. M. (2010). A regional comparison of particle size distributions and the power law approximation in oceanic and estuarine surface waters. *J. Geophys. Res.* 115, C10028. doi: 10.1029/2010JC006256

Carranza, M. M., Gille, S. T., Franks, P. J. S., Johnson, K. S., Pinkel, R., and Girton, J. B. (2018). When mixed layers are not mixed. Storm-driven mixing and bio-optical vertical gradients in mixed layers of the southern ocean. *J. Geophysical Research: Oceans* 123, 7264–7289. doi: 10.1029/2018JC014416

Cavan, E. L., Trimmer, M., Shelley, F., and Sanders, R. (2017). Remineralization of particulate organic carbon in an ocean oxygen minimum zone. *Nat. Commun.* 8, 14847. doi: 10.1038/ncomms14847

Cetinić, I., Perry, M. J., Briggs, N. T., Kallin, E., D'Asaro, E. A., and Lee, C. M. (2012). Particulate organic carbon and inherent optical properties during 2008 North Atlantic Bloom Experiment. *J. Geophysical Research: Oceans* 117. doi: 10.1029/2011JC007771

Clements, D. J., Yang, S., Weber, T., McDonnell, A. M. P., Kiko, R., Stemmann, L., et al. (2022). Constraining the particle size distribution of large marine particles in the global ocean with in situ optical observations and supervised learning. *Global Biogeochemical Cycles* 36, e2021GB007276. doi: 10.1029/2021GB007276

Falkowski, P. G., Barber, R. T., and Smetacek, V. (1998). Biogeochemical controls and feedbacks on ocean primary production. *Science* 281, 200–206. doi: 10.1126/science.281.5374.200

Fawcett, S., and Forrer, H. (2020). Particulate organic carbon concentration in seawater profiles collected on board the R/V Akademik Tryoshnikov in the Southern Ocean during the austral summer of 2016/2017 as part of the Antarctic Circumnavigation Expedition (ACE). *Zenodo*. doi: 10.5281/zenodo.3706710

Garcia, C. A. E., Garcia, V. M. T., and McClain, C. R. (2005). Evaluation of SeaWiFS chlorophyll algorithms in the Southwestern Atlantic and Southern Oceans. *Remote Sens. Environ.* 95, 125–137. doi: 10.1016/j.rse.2004.12.006

Graff, J. R., Westberry, T. K., Milligan, A. J., Brown, M. B., Dall'Olmo, G., Dongen-Vogels, V., et al. (2015). Analytical phytoplankton carbon measurements spanning diverse ecosystems. *Deep Sea Res. Part I: Oceanographic Res. Papers* 102, 16–25. doi: 10.1016/j.dsr.2015.04.006

Gruber, N., Gloor, M., Mikaloff Fletcher, S. E., Doney, S. C., Dutkiewicz, S., Follows, M. J., et al. (2009). Oceanic sources, sinks, and transport of atmospheric CO2. *Global Biogeochemical Cycles* 23. doi: 10.1029/2008GB003349

Hirawake, T., Takao, S., Horimoto, N., Ishimaru, T., Yamaguchi, Y., and Fukuchi, M. (2011). A phytoplankton absorption-based primary productivity model for remote sensing in the Southern Ocean. *Polar Biol.* 34, 291–302. doi: 10.1007/s00300-010-0949-y

Hooker, S. B., and Zibordi, G. (2005). Advanced methods for characterizing the immersion factor of irradiance sensors. *J. Atmos. Oceanic Technol.* 22, 757–770. doi: 10.1175/JTECH1736.1

Huot, Y., Morel, A., Twardowski, M. S., Stramski, D., and Reynolds, R. A. (2008). Particle optical backscattering along a chlorophyll gradient in the upper layer of the eastern South Pacific Ocean. *Biogeosciences* 5, 495–507. doi: 10.5194/bg-5-495-2008

Jackson, G. A. (1980). Phytoplankton growth and Zooplankton grazing in oligotrophic oceans. *Nature* 284, 439–441. doi: 10.1038/284439a0

Jackson, G. A., and Burd, A. B. (1998). Aggregation in the marine environment. *Environ. Sci. Technol.* 32, 2805–2814. doi: 10.1021/es980251w

Jena, B. (2017). The effect of phytoplankton pigment composition and packaging on the retrieval of chlorophyll-a concentration from satellite observations in the Southern Ocean. *Int. J. Remote Sens.* 38, 3763–3784. doi: 10.1080/01431161.2017.1308034

Johnson, K. S., Plant, J. N., Coletti, L. J., Jannasch, H. W., Sakamoto, C. M., Riser, S. C., et al. (2017). Biogeochemical sensor performance in the SOCCOM profiling float array. *J. Geophysical Research: Oceans* 122, 6416–6436. doi: 10.1002/2017JC012838

Johnson, R., Strutton, P. G., Wright, S. W., McMinn, A., and Meiners, K. M. (2013). Three improved satellite chlorophyll algorithms for the Southern Ocean. *J. Geophysical Research: Oceans* 118, 3694–3703. doi: 10.1002/jgrc.20270

Jonasz, M., and Fournier, G. R. (2011). *Light Scattering by Particles in Water: Theoretical and Experimental Foundations*. (Elsevier). doi: 10.1016/B978-0-12-388751-1.X5000-5

Kahru, M., and Mitchell, B. G. (2010). Blending of ocean colour algorithms applied to the Southern Ocean. *Remote Sens. Lett.* 1, 119–124. doi: 10.1080/01431160903547940

Karakuş, O., Völker, C., Iversen, M., Hagen, W., and Hauck, J. (2022). The role of zooplankton grazing and nutrient recycling for global ocean biogeochemistry and phytoplankton phenology. *J. Geophysical Research: Biogeosciences* 127, e2022JG006798. doi: 10.1029/2022JG006798

Kinsman, S. (2018). "Particle Size Instrumentation — Coulter® Counter," in *Particle Characterization in Technology*. Ed. J. K. Beddow (Boca Raton: CRC Press), 183–186. doi: 10.1201/9781351075350-9

Loisel, H., Bosc, E., Stramski, D., Oubelkheir, K., and Deschamps, P.-Y. (2001). Seasonal variability of the backscattering coefficient in the Mediterranean Sea based on satellite SeaWiFS imagery. *Geophysical Res. Lett.* 28, 4203–4206. doi: 10.1029/2001GL013863

Maffione, R. A., and Dana, D. R. (1997). Instruments and methods for measuring the backward-scattering coefficient of ocean waters. *Appl. Optics* 36, 6057–6067. doi: 10.1364/AO.36.006057

Marrari, M., Hu, C., and Daly, K. (2006). Validation of SeaWiFS chlorophyll a concentrations in the Southern Ocean: A revisit. *Remote Sens. Environ.* 105, 367–375. doi: 10.1016/j.rse.2006.07.008

Martinez-Vicente, V., Dall'Olmo, G., Tarran, G., Boss, E., and Sathyendranath, S. (2013). Optical backscattering is correlated with phytoplankton carbon across the Atlantic Ocean. *Geophys. Res. Lett.* 40, 1154–1158. doi: 10.1002/grl.50252

Mignot, A., Ferrari, R., and Claustre, H. (2018). Floats with bio-optical sensors reveal what processes trigger the North Atlantic bloom. *Nat. Commun.* 9, 190. doi: 10.1038/s41467-017-02143-6

Morel, A., and Gentili, B. (2009). A simple band ratio technique to quantify the colored dissolved and detrital organic material from ocean color remotely sensed data. *Remote Sens. Environ.* 113, 998–1011. doi: 10.1016/j.rse.2009.01.008

Morel, A., and Maritorena, S. (2001). Bio-optical properties of oceanic waters: A reappraisal. *J. Geophys. Res.* 106, 7163–7180. doi: 10.1029/2000JC000319

Moutier, W., Thomalla, S., Bernard, S., Wind, G., Ryan-Keogh, T., and Smith, M. (2019). Evaluation of chlorophyll-a and POC MODIS aqua products in the southern ocean. *Remote Sens.* 11, 1793. doi: 10.3390/rs11151793

Park, Y.-H., Park, T., Kim, T.-W., Lee, S.-H., Hong, C.-S., Lee, J.-H., et al. (2019). Observations of the antarctic circumpolar current over the udintsev fracture zone, the narrowest choke point in the southern ocean. *J. Geophysical Research: Oceans* 124, 4511–4528. doi: 10.1029/2019JC015024

Pereira, E. S., and Garcia, C. A. E. (2018). Evaluation of satellite-derived MODIS chlorophyll algorithms in the northern Antarctic Peninsula. *Deep Sea Res. Part II: Topical Stud. Oceanography* 149, 124–137. doi: 10.1016/j.dsr2.2017.12.018

Picheral, M., Guidi, L., Stemmann, L., Karl, D. M., Iddaoud, G., and Gorsky, G. (2010). The Underwater Vision Profiler 5: An advanced instrument for high spatial resolution studies of particle size spectra and zooplankton. *Limnology Oceanography: Methods* 8, 462–473. doi: 10.4319/lom.2010.8.462

Ras, J., Claustre, H., and Uitz, J. (2008). Spatial variability of phytoplankton pigment distributions in the Subtropical South Pacific Ocean: comparison between in situ and predicted data. *Biogeosciences* 5, 353–369. doi: 10.5194/bg-5-353-2008

Reynolds, R. A., Stramski, D., and Neukermans, G. (2016). Optical backscattering by particles in Arctic seawater and relationships to particle mass concentration, size distribution, and bulk composition: Particle backscattering in Arctic seawater. *Limnol. Oceanogr* 61, 1869–1890. doi: 10.1002/lno.10341

Robinson, C. M., Huot, Y., Schuback, N., Ryan-Keogh, T. J., Thomalla, S. J., and Antoine, D. (2021). High latitude Southern Ocean phytoplankton have distinctive bio-optical properties. *Opt. Express* 29, 21084–21112. doi: 10.1364/OE.426737

Roesler, C., Uitz, J., Claustre, H., Boss, E., Xing, X., Organelli, E., et al. (2017). Recommendations for obtaining unbiased chlorophyll estimates from in situ chlorophyll fluorometers: A global analysis of WET Labs ECO sensors. *Limnology Oceanography: Methods* 15, 572–585. doi: 10.1002/lom3.10185

Sarmiento, J. L., Johnson, K. S., Arteaga, L. A., Bushinsky, S. M., Cullen, H. M., Gray, A. R., et al. (2023). The Southern Ocean carbon and climate observations and modeling (SOCCOM) project: a review. *Prog. Oceanogr.* 219, 103130. doi: 10.1016/j.pocean.2023.103130

Sathyendranath, S., Platt, T., and Forget, M.-H. (2007). "Oceanic Primary Production: Comparison of Models," in *OCEANS 2007*. (Europe, Aberdeen, UK. (IEEE), 1–3. doi: 10.1109/OCEANSE.2007.4302468

Sathyendranath, S., Stuart, V., Nair, A., Oka, K., Nakane, T., Bouman, H., et al. (2009). Carbon-to-chlorophyll ratio and growth rate of phytoplankton in the sea. *Mar. Ecol. Prog. Ser.* 383, 73–84. doi: 10.3354/meps07998

Schallenberg, C., Harley, J. W., Jansen, P., Davies, D. M., and Trull, T. W. (2019). Multi-year observations of fluorescence and backscatter at the southern ocean time series (SOTS) shed light on two distinct seasonal bio-optical regimes. *Front. Mar. Sci.* 6. doi: 10.3389/fmars.2019.00595

Schallenberg, C., Strzepek, R. F., Bestley, S., Wojtasiewicz, B., and Trull, T. W. (2022). Iron limitation drives the globally extreme fluorescence/chlorophyll ratios of the southern ocean. *Geophysical Res. Lett.* 49, e2021GL097616. doi: 10.1029/2021GL097616

Slade, W. H., Boss, E., and Russo, C. (2011). Effects of particle aggregation and disaggregation on their inherent optical properties. *Opt. Express* 19, 7945–7959. doi: 10.1364/OE.19.007945

Stark, J. S., Raymond, T., Deppeler, S. L., and Morrison, A. K. (2019). "Chapter 1 - Antarctic Seas," in *World Seas: an Environmental Evaluation (Second Edition)*. Ed. C. Sheppard (Cambridge, Massachusetts: Academic Press), 1–44. doi: 10.1016/B978-0-12-805068-2.00002-4

Steinberg, D. K., and Landry, M. R. (2017). Zooplankton and the ocean carbon cycle. *Annu. Rev. Mar. Sci.* 9, 413–444. doi: 10.1146/annurev-marine-010814-015924

Stramska, M., Stramski, D., Hapter, R., Kaczmarek, S., and Stoń-Egiert, J. (2003). Bio-optical relationships and ocean color algorithms for the north polar region of the Atlantic. *J. Geophys. Res.* 108, 3143. doi: 10.1029/2001JC001195

Stramski, D., Reynolds, R. A., Babin, M., Kaczmarek, S., Lewis, M. R., Röttgers, R., et al. (2008). Relationships between the surface concentration of particulate organic carbon and optical properties in the eastern South Pacific and eastern Atlantic Oceans. *Biogeosciences* 5, 171–201. doi: 10.5194/bg-5-171-2008

Stramski, D., Reynolds, R. A., Kahru, M., and Mitchell, B. G. (1999). Estimation of particulate organic carbon in the ocean from satellite remote sensing. *Science* 285, 239–242. doi: 10.1126/science.285.5425.239

Szeto, M., Werdell, P. J., Moore, T. S., and Campbell, J. W. (2011). Are the world's oceans optically different? *J. Geophysical Research: Oceans* 116. doi: 10.1029/2011JC007230

Thomalla, S. J., Ogunkoya, A. G., Vichi, M., and Swart, S. (2017). Using optical sensors on gliders to estimate phytoplankton carbon concentrations and chlorophyll-to-carbon ratios in the southern ocean. *Front. Mar. Sci.* 4. doi: 10.3389/fmars.2017.00034

Turner, J. T. (2015). Zooplankton fecal pellets, marine snow, phytodetritus and the ocean's biological pump. *Prog. Oceanography* 130, 205–248. doi: 10.1016/j.pocean.2014.08.005

Uchida, T., Balwada, D., Abernathey, R., Prend, C. J., Boss, E., and Gille, S. T. (2019). Southern ocean phytoplankton blooms observed by biogeochemical floats. *J. Geophysical Research: Oceans* 124, 7328–7343. doi: 10.1029/2019JC015355

Walton, D. W. H., and Thomas, J. (2018). *Cruise report - antarctic circumnavigation expedition (ACE) 20th december 2016 - 19th march 2017*. doi: 10.5281/zenodo.1443511

Wynn-Edwards, C., Davies, D. M., Jansen, P., Bray, S. G., Eriksen, R., and Trull, T. W. (2019). *IMOS-Southern Ocean Time Series (SOTS)-Annual Reports: 2012/2013*. (Australian Integrated Marine Observing System, University of Tasmania).

Zhang, Y. L., Liu, M. L., Wang, X., Zhu, G. W., and Chen, W. M. (2009). Bio-optical properties and estimation of the optically active substances in Lake Tianmuhu in summer. *Int. J. Remote Sens.* 30, 2837–2857. doi: 10.1080/01431160802558592